

Factorized Diffusion Architectures for Unsupervised Image Generation and Segmentation

Xin Yuan
University of Chicago
yuanx@uchicago.edu

Michael Maire
University of Chicago
mmaire@uchicago.edu

Abstract

We develop a neural network architecture which, trained in an unsupervised manner as a denoising diffusion model, simultaneously learns to both generate and segment images. Learning is driven entirely by the denoising diffusion objective, without any annotation or prior knowledge about regions during training. A computational bottleneck, built into the neural architecture, encourages the denoising network to partition an input into regions, denoise them in parallel, and combine the results. Our trained model generates both synthetic images and, by simple examination of its internal predicted partitions, a semantic segmentation of those images. Without any finetuning, we directly apply our unsupervised model to the downstream task of segmenting real images via noising and subsequently denoising them. Experiments demonstrate that our model achieves accurate unsupervised image segmentation and high-quality synthetic image generation across multiple datasets.

1. Introduction

Supervised deep learning yields powerful discriminative representations, and has fundamentally advanced many computer vision tasks, including image classification [12, 19, 26, 55], object detection [16, 38, 46], and semantic and instance segmentation [20, 31, 39]. Yet, annotation efforts [12], especially those involving fine-grained labeling for tasks such as segmentation [37], can become prohibitively expensive to scale with increasing dataset size. This motivates an ongoing revolution in self-supervised methods for visual representation learning, which do not require any annotated data during a large-scale pre-training phase [6, 9, 11, 14, 21, 33, 63]. However, many of these approaches, including those in the particularly successful contrastive learning paradigm [9, 11, 21], still require supervised fine-tuning (*e.g.*, linear probing) on labeled data to adapt networks to downstream tasks such as classification [9, 21] or segmentation [7, 65].

In parallel with the development of self-supervised deep learning, rapid progress on a variety of frameworks for deep generative models [17, 25, 30, 35, 47, 56, 57, 61, 62] has led to new systems for high-quality image synthesis. This progress inspires efforts to explore representation learning within generative models, with recent results suggesting that image generation can serve as a good proxy task for capturing high-level semantic information, while also enabling realistic image synthesis.

Building upon generative adversarial networks (GANs) [17] or variational autoencoders (VAEs) [30], InfoGAN [10] and Deep InfoMax [24] demonstrate that generative models can perform image classification without any supervision. PerturbGAN [4] focuses on a more complex task, unsupervised image segmentation, by forcing an encoder to map an image to the input of a pre-trained generator so that it synthesizes a composite image that matches the original input image. However, here training is conducted in two stages and mask generation relies on knowledge of predefined object classes.

Denoising diffusion probabilistic models (DDPMs) [25] also achieve impressive performance in generating realistic images. DatasetDDPM [2] investigates the intermediate activations from the pre-trained U-Net [48] network that approximates the Markov step of the reverse diffusion process in DDPM, and proposes a simple semantic segmentation pipeline fine-tuned on a few labeled images. In spite of this usage of labels, DatasetDDPM demonstrates that high-level semantic information, which is valuable for downstream vision tasks, can be extracted from pre-trained DDPM U-Net. Diff-AE [45] and PADE [66] are recently proposed methods for representation learning by reconstructing images in the DDPM framework. However, their learned representations are in the form of a latent vector containing information applicable for image classification.

In contrast to all of these methods, we demonstrate a fundamentally new paradigm for unsupervised visual representation learning with generative models: constrain the architecture of the model with a structured bottleneck that provides an interpretable view of the generation process, and

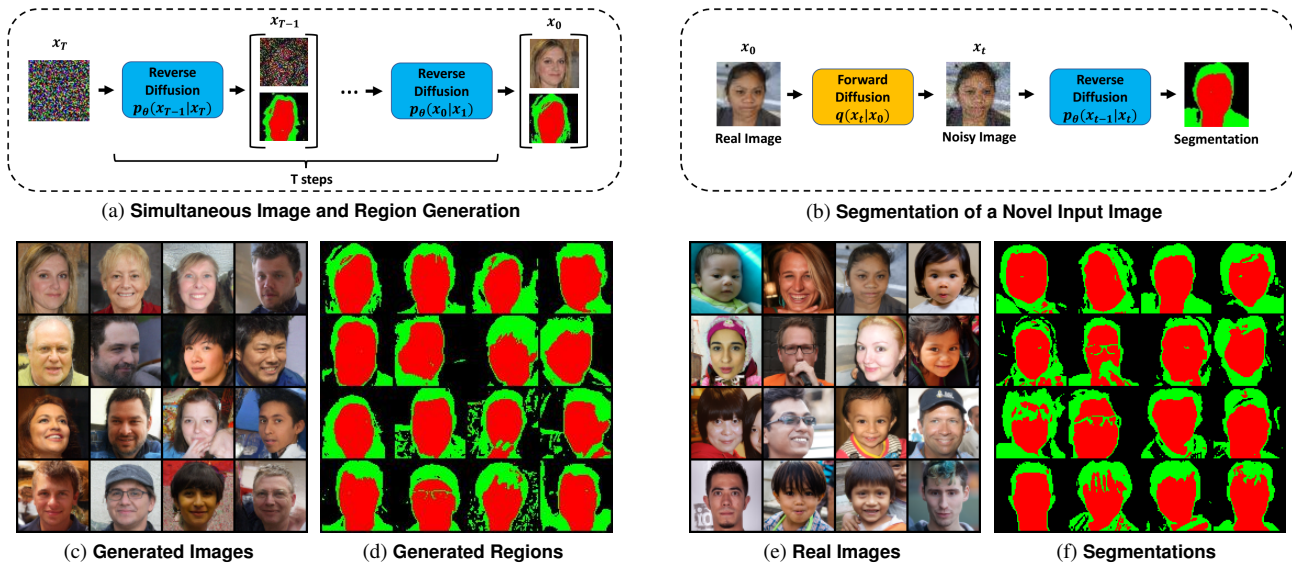


Figure 1. **Unifying image generation and segmentation.** (a) We design a denoising diffusion model with a specific architecture that couples region prediction with spatially-masked diffusion over predicted regions, thereby generating both simultaneously. (b) An additional byproduct of running our trained denoising model on an arbitrary input image is a segmentation of that image. Using a model trained on FFHQ [29], we achieve both high quality synthesis of images and corresponding semantic segmentations (c-d), as well as the ability to accurately segment images of real faces (e-f). Segmenting a real image is fast, requiring only one forward pass (one denoising step).

from which one can simply read off desired latent information. This structured bottleneck does not exist in isolation, but rather is co-designed alongside the network architecture preceding and following it. The computational layout of these pieces must work together in a manner that forces the network, when trained from scratch for generation alone, to populate the bottleneck data structure with an interpretable visual representation.

We demonstrate this concept in the scenario of a DDPM for image generation and the selection of semantic segmentation as the interpretable representation to be read from the bottleneck. Thus, we frame unsupervised image segmentation and generation in a unified system. Moreover, experiments demonstrate that domain-specific bottleneck design not only allows us to accomplish an end task (segmentation) for free, but also boosts the quality of generated samples. This challenges the assumption that generic architectures (e.g., Transformers) alone suffice; we find synergy by organizing such generic building blocks into a factorized architecture which generates different image regions in parallel.

Figure 1 provides an overview of our setting alongside example results, while Figure 2 illustrates the details of our DDPM architecture which are fully presented in Section 3. This architecture constrains the computational resources available for denoising in a manner that encourages learning of a factorized model of the data. Specifically, each step of the DDPM has the ability to utilize additional inference passes through multiple copies of a subnetwork if it is willing to decompose the denoising task into parallel sub-

problems. The specific decomposition strategy itself must be learned, but, by design, is structured in a manner that reveals the solution to our target task of image segmentation. We summarize our contributions as three-fold:

- **Unified learning of generation and segmentation.** We train our new DDPM architecture once, obtaining a model directly applicable to two different tasks with zero modification or fine-tuning: image generation and image segmentation. Segmenting a novel input image is fast, comparable in speed to any system using a single forward pass of a U-Net [48] like architecture.
- **Unsupervised segmentation for free.** Our method automatically learns meaningful regions (e.g., foreground and background), guided only by the DDPM denoising objective; no extra regularization terms, no use of labels.
- **Higher quality image synthesis.** Our model generates higher-quality images than the baseline DDPM, as well as their corresponding segmentations simultaneously. We achieve excellent quantitative and qualitative results under common evaluation protocols (Section 4).

Beyond improvements to image generation and segmentation, our work can be viewed as the first case study of a new paradigm for using generation as a learning objective, in combination with model architecture as a constraint. Rather than viewing a pre-trained generative model as a source from which to extract and repurpose features for downstream tasks, design the model architecture in the first place so that, as a byproduct of training from scratch to generate, it also learns to perform the desired task.

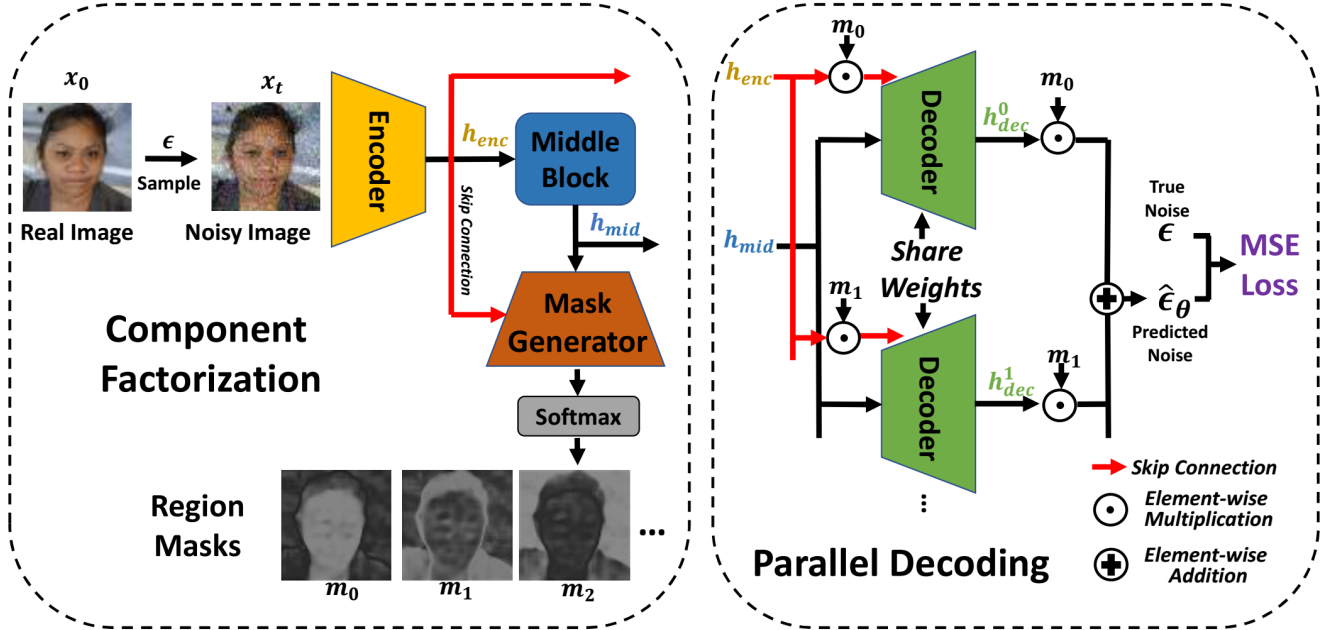


Figure 2. **Factorized diffusion architecture.** Our framework restructures the architecture of the neural network within a DDPM [25] so as to decompose the image denoising task into parallel subtasks. All modules are end-to-end trainable and optimized according to the same denoising objective as DDPM. **Left: Component factorization.** An *Encoder*, equivalent to the first half of a standard DDPM U-Net architecture, extracts features h_{enc} . A common *Middle Block* processes *Encoder* output into shared latent features h_{mid} . Note that *Middle Block* and h_{mid} exist in the standard denoising DDPM U-Net by default. We draw it as a standalone module for a better illustration of the detailed architectural design. A *Mask Generator*, structured as the second half of a standard U-Net receives h_{mid} as input, alongside all encoder features h_{enc} injected via skip connections to layers of corresponding resolution. This later network produces a soft classification of every pixel into one of K region masks, m_0, m_1, \dots, m_K . **Right: Parallel decoding.** A *Decoder*, also structured as the second half of a standard U-Net, runs separately for each region. Each instance of the *Decoder* receives shared features h_{mid} and a masked view of encoder features $h_{enc} \odot m_i$ injected via skip connections to corresponding layers. Decoder outputs are masked prior to combination. Though not pictured, we inject timestep embedding t into the *Encoder*, *Mask Generator*, and *Decoder*.

2. Related Work

Image Segmentation. Generic segmentation, which seeks to partition an image into meaningful regions without prior knowledge about object categories present in the scene, is a longstanding challenge for computer vision. Early methods rely on combinations of hand-crafted features based on intensity, color, and texture cues [5, 41], clustering algorithms [54], and a duality between closed contours and the regions they bound [1]. Deep learning modernized the feature representations used in these pipelines, yielding systems which, trained with supervision from annotated regions [40], reach near human-level accuracy on predicting and localizing region boundaries [3, 32, 53, 60].

Semantic segmentation, which assigns a category label to each pixel location in image, has been similarly revolutionized by deep learning. Here, the development of specific architectures [18, 39, 48] enabled porting of approaches for image classification to the task of semantic segmentation.

Recent research has refocused on the challenge of learning to segment without reliance on detailed annotation for

training. Hwang *et al.* [27] combine two sequential clustering modules for both pixel-level and segment-level to perform this task. Ji *et al.* [28] and Ouali *et al.* [43] follow the concept of mutual information maximization to partition pixels into two segments. Savarese *et al.* [51] further propose a learning-free adversarial method from the information theoretic perspective, with the goal of minimizing predictability among different pixel subsets.

Segmentation Learning in Generative Models. Generative model-based approaches produce a semantic mask by perturbing [4] or redrawing [8] the generated foreground and background masks. Despite good performance, these methods apply only to two-class partitions and require extra loss terms based upon object priors in training datasets.

Denoising diffusion probabilistic models (DDPMs) [25] achieve state-of-the-art performance in generating realistic images. The incremental nature of their training process may offer advantages for scaling up models in a stable manner. A few recent works [2, 45, 66] explore representation learning capability in DDPMs. DatasetDDPM [2] is the first to explore the few-shot segmentation in pre-trained diffu-

sion models. This method still requires human labels to train a linear classifier. Moreover, with the default U-Net architecture [48], it loses the efficiency and flexibility of generating image and masks in a single-stage manner. Diff-AE [45] and PADE [66] perform representation learning driven by a reconstruction objective in the DDPM framework. Unfortunately, their learned latent vector is not applicable to more challenging segmentation tasks. Additionally, their learned representations require an extra pre-trained interpreter to perform downstream image classification.

DiffuMask [59] takes a pre-trained Stable Diffusion model [47], which is trained with large-scale text-to-image datasets (and thus solves a far less challenging problem), and conducts a post-hoc investigation on how to extract segmentation from its attention maps. Neither our system, nor the baseline DDPM to which we compare, makes use of such additional information. Furthermore, DiffuMask does not directly output segmentation; it is basically a dataset generator, which produces generated images and pseudo labels, which are subsequently used to train a separate segmentation model. Our method, in contrast, is both completely unsupervised and provides an end-to-end solution by specifying an architectural design in which training to generate reveals segmentations as a bonus.

MAGE [36] shares with us a similar motivation of framing generation and representation learning in a unified framework. However, our approach is distinct in terms of both (1) task: we tackle a more complex unsupervised segmentation task (without fine-tuning) instead of image classification (with downstream fine-tuning), and (2) design: ‘masks’ play a fundamentally different role in our system. MAGE adopts an MAE [22]-like masking scheme on input data, in order to provide a proxy reconstruction objective for self-supervised representation learning. Our use of region masks serves a different purpose, as they are integral components of the model being learned and facilitate factorization of the image generation process into parallel synthesis of different segments.

3. Factorized Diffusion Models

Figure 2 illustrates the overall architecture of our system, which partitions the denoising network within a diffusion model into an unsupervised region mask generator and parallel per-region decoders.

3.1. Unsupervised Region Factorization

To simultaneously learn representations for both image generation and unsupervised segmentation, we first design the region mask generator based on the first half (encoder) of a standard DDPM U-Net. We obtain input \mathbf{x}_t , a noised ver-

sion of \mathbf{x}_0 , via forward diffusion:

$$\begin{aligned} q(\mathbf{x}_t|\mathbf{x}_0) &:= \mathcal{N}(\mathbf{x}_t; \sqrt{\bar{\alpha}_t}\mathbf{x}_0, (1 - \bar{\alpha}_t)I), \\ \mathbf{x}_t &= \sqrt{\bar{\alpha}_t}\mathbf{x}_0 + \sqrt{1 - \bar{\alpha}_t}\boldsymbol{\epsilon}, \boldsymbol{\epsilon} \sim \mathcal{N}(0, 1), \end{aligned} \quad (1)$$

where $\alpha_t = 1 - \beta_t$, $\bar{\alpha}_t = \prod_{s=1}^t \alpha_s$.

In addition to the encoder half of the U-Net, we instantiate a middle block consisting of layers operating on lower spatial resolution features. Parameterizing these subnetworks as θ_{enc} and θ_{mid} , we extract latent representations:

$$\mathbf{h}_{enc} = \theta_{enc}(\mathbf{x}_t, t), \quad (2)$$

$$\mathbf{h}_{mid} = \theta_{mid}(\mathbf{h}_{enc}, t) \quad (3)$$

where \mathbf{h}_{enc} encapsulates features at all internal layers of θ_{enc} , for subsequent use as inputs, via skip connections, to corresponding layers of decoder-style networks (second half of a standard U-Net).

We instantiate a mask generator, θ_{mask} , as one such decoder-style subnetwork. A softmax layer produces an output tensor with K channels, representing K different regions in image \mathbf{x}_0 :

$$\mathbf{m}_k = \theta_{mask}(\mathbf{h}_{mid}, \mathbf{h}_{enc}, t) \quad (4)$$

Following a U-Net architecture, \mathbf{h}_{enc} feeds into θ_{mask} through skip-connections.

3.2. Parallel Decoding Through Weight Sharing

We aim to extend a standard DDPM U-Net decoder θ_{dec} to consider region structure during generation. One simple design is to condition on $\mathbf{m} = \{\mathbf{m}_0, \mathbf{m}_1, \dots\}$ by concatenating it with input \mathbf{h}_{mid} and \mathbf{h}_{enc} along the channel dimension:

$$\hat{\boldsymbol{\epsilon}} = \theta_{dec}(\text{concat}[\mathbf{h}_{mid}, \mathbf{m}], \text{concat}[\mathbf{h}_{enc}, \mathbf{m}], t), \quad (5)$$

where \mathbf{h}_{mid} and \mathbf{h}_{enc} are generated from Eq. 2 and Eq. 3. We downsample \mathbf{m} accordingly to the same resolution as \mathbf{h}_{mid} and \mathbf{h}_{enc} at different stages. However, such a design significantly modifies (*e.g.*, channel sizes) the original U-Net decoder architecture. Moreover, conditioning with the whole mask representation may also result in a trivial solution that simply ignores region masks.

To address these issues, we separate the decoding scheme into multiple parallel branches of weight-shared U-Net decoders, each masked by a single segment. Noise prediction for k -th branch is:

$$\hat{\boldsymbol{\epsilon}}_k = \theta_{dec}(\mathbf{h}_{mid}, \mathbf{h}_{enc} \odot \mathbf{m}_k, t) \quad (6)$$

and the output is a sum of region-masked predictions:

$$\hat{\boldsymbol{\epsilon}} = \sum_{k=0}^{K-1} \hat{\boldsymbol{\epsilon}}_k \odot \mathbf{m}_k \quad (7)$$

Algorithm 1

Training Masked Diffusion

Input: Data \mathbf{x}_0
Output: Trained model θ
Initialize:
 Model weights θ ,
 Timesteps T
for iter = 1 **to** Iter_{total} **do**
 Sample $t \in [1, T]$
 Sample \mathbf{x}_t using Eq. 1
 Calculate $\hat{\epsilon}$ using Eq. 7
 Backprop with Eq. 8.
 Update θ .
end for
 return θ

Algorithm 2

Image and Mask Generation

Input: Noise \mathbf{x}_T , trained model θ
Output:
 Image $\hat{\mathbf{x}}_0$ and segmentation $\hat{\mathbf{m}}_0$
Initialize: $\mathbf{x}_T \sim \mathcal{N}(0, 1)$
for $t = T$ **to** 1 **do**
 Sample \mathbf{z} using Eq. 10
 Perform reversed diffusion using
 Eq. 9
if $t = 1$ **then**
 collect $\hat{\mathbf{m}}_0$ using Eq. 4
 return $\hat{\mathbf{x}}_0$ and $\hat{\mathbf{m}}_0$.
end if
end for

3.3. Optimization with Denoising Objective

We train our model in an end-to-end manner, driven by the simple DDPM denoising objective. Model weights $\theta = \{\theta_{enc}, \theta_{mid}, \theta_{dec}, \theta_{mask}\}$ are optimized by minimizing the noise prediction loss:

$$L = \mathbb{E} \|\epsilon - \hat{\epsilon}\|_2^2 \quad (8)$$

Unlike previous work, our method does not require a mask regularization loss term [4, 8, 51], which pre-defines mask priors (e.g., object size). Algorithm 1 summarizes training.

3.4. Segmentation via Reverse Diffusion

Once trained, we can deploy our model to both segment novel input images as well as synthesize images from noise.

Real Image Segmentation. Given clean input image \mathbf{x}_0 , we first sample a noisy version \mathbf{x}_t through forward diffusion in Eq. 1. We then perform one-step denoising by passing \mathbf{x}_t to the model. We collect the predicted region masks as the segmentation for \mathbf{x}_0 using Eq. 4.

Image and Mask Generation. Using reverse diffusion, our model can generate realistic images and their corresponding segmentation masks, starting from a pure noise input $\mathbf{x}_T \sim \mathcal{N}(0, 1)$. Reverse diffusion predicts \mathbf{x}_{t-1} from \mathbf{x}_t :

$$\mathbf{x}_{t-1} = 1/\sqrt{\alpha_t}(\mathbf{x}_t - \frac{1 - \alpha_t}{\sqrt{1 - \alpha_t}}\theta(\mathbf{x}_t, t)) + \sigma_t \mathbf{z}, \quad (9)$$

$$\mathbf{z} \sim \mathcal{N}(0, 1) \quad \text{if } t > 1 \quad \text{else } \mathbf{z} = 0. \quad (10)$$

where σ_t is empirically set according to the DDPM noise scheduler. We perform T steps of reverse diffusion to generate an image. We also collect its corresponding mask using Eq. 9 when $t = 1$. Algorithm 2 summarizes this process.

4. Experiments

We evaluate on: (1) real image segmentation, (2) image and region mask generation, using Flower [42], CUB [58], FFHQ [29], CelebAMask-HQ [34], and ImageNet [50].

Evaluation Metrics. For unsupervised segmentation on Flower and CUB, we follow the data splitting in IEM [51] and evaluate predicted mask quality under three commonly used metrics, denoted as Acc., IOU and DICE score [8, 51]. Acc. is the (per-pixel) mean accuracy of the foreground prediction. IOU is the predicted foreground region’s intersection over union (IoU) with the ground-truth foreground region. DICE score is defined as $2 \frac{\hat{F} \cap F}{|\hat{F}|}$ [13]. On ImageNet, we evaluate our method on Pixel-ImageNet [64], which provides human-labeled segmentation masks for 0.485M images covering 946 object classes. We report Acc., IOU and DICE score on a randomly sampled subset, each class containing at most 20 images. For face datasets, we train our model on FFHQ and only report per-pixel accuracy on the CelebAMask test set, using provided ground-truth.

For image and mask generation, we use Fréchet Inception Distance (FID) [23] for generation quality assessment. Since we can not obtain the ground-truth for generated masks, we apply a supervised U-Net segmentation model, pre-trained on respective datasets, to the generated images and measure the consistency between masks in terms of per-pixel accuracy. In addition to quantitative comparisons, we show extensive qualitative results.

Implementation Details. We train Flower, CUB and Face models at both 64×64 and 128×128 resolution. We also train class-conditioned ImageNet models with 64×64 resolution. For all experiments, we use the U-Net [48] encoder-middle-decoder architecture similar to [25]. We use the decoder architecture as our mask generator and set the number of factorized masks K as 3. For 64×64 the architecture is as follows: The downsampling stack performs four steps of downsampling, each with 3 residual blocks. The upsampling stack is setup as a mirror image of the downsampling stack. From highest to lowest resolution, U-Net stages use $[C, 2C, 3C, 4C]$ channels, respectively. For 128×128 architecture, the down/up sampling block is 5-step with $[C, C, 2C, 3C, 4C]$ channels, each with two residual blocks, respectively. We set $C = 128$ for all models.

We use Adam to train all the models with a learning rate of 10^{-4} and an exponential moving average (EMA) over model parameters with rate 0.9999. For all datasets except ImageNet, we train 64×64 and 128×128 models on 8 and 32 Nvidia V100 32GB GPUS, respectively. For Flower, CUB and FFHQ, we train the models for 50K, 50K, 500K iterations with batch size of 128, respectively. For ImageNet, we train 500K iterations on 32 Nvidia V100 GPUS with batch size 512. We adopt the linear noise scheduler as in Ho *et al.* [25] with $T = 1000$ timesteps.

4.1. Image Segmentation

To evaluate our method on real image segmentation, we set t as 30 for forward diffusion process. For Flower and CUB, Figures 3 and 4 show test images and predicted segmenta-

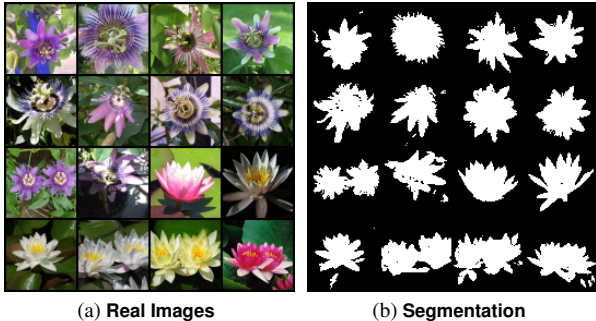


Figure 3. Segmentation on Flower.

Methods	Acc.	IOU	DICE
GrabCut [49]	82.0	69.2	79.1
ReDO [8]	87.9	76.4	-
IEM [51]	88.3	76.8	84.6
IEM+SegNet [51]	89.6	78.9	86.0
Ours	90.1	79.7	87.2

Table 1. Comparisons on Flower.

tions. Tables 1 and 2 provide quantitative comparison with representative unsupervised image segmentation methods: GrabCut [49], ReDO [8] and IEM [51]. As shown in Table 1 and Table 2, our method outperforms all competitors.

We also visualize the predicted face parsing results on FFHQ and CelebAMask datasets in Figure 1(c)(d) and Figure 5. Our model learns to accurately predict three segments corresponding to semantic components: skin, hair, and background. This particular semantic partitioning emerges from our unsupervised learning objective, without any additional prior. With ground-truth provided on CelebAMask-HQ, we also compare the pixel accuracy and mean of IOU with a supervised U-Net and DatasetDDPM [2]. For the former, we train a supervised segmentation model with 3-class cross-entropy loss. For the unsupervised setting, we perform K-means ($K=3$) on the pre-trained DDPM, denoted as DatasetDDPM-unsup. Table 3 shows that we outperform DatasetDDPM by a large margin and achieve a relatively small performance gap with a supervised U-Net.

Figure 6 shows the accurate segmentation results for ImageNet classes: ostrich, pekinese, papillon, and tabby. We compare with supervised U-Net and DatasetDDPM-unsup in Table 4. We show more visualizations in Appendix Section 6.2.

4.2. Image and Mask Generation

We evaluate our method on image and mask generation. As shown in Figure 7, 8, 1(c)(d) and 11, our method is able to generate realistic images. In the upper row of Table 5, we see a consistent quality improvement over the original DDPM. This suggests our method as a better architecture than standard U-Net through separating computational

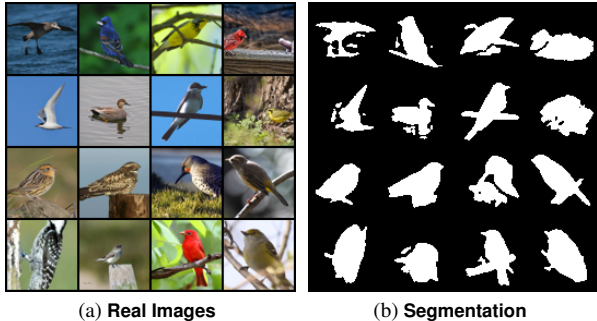


Figure 4. Segmentation on CUB.

Methods	Acc.	IOU	DICE
GrabCut [49]	72.3	36.0	48.7
PerturbGAN [4]	-	38.0	-
ReDO [8]	84.5	42.6	-
IEM [51]	88.6	52.2	66.0
IEM+SegNet [51]	89.3	55.1	68.7
Ours	89.6	56.1	69.4

Table 2. Comparisons on CUB.

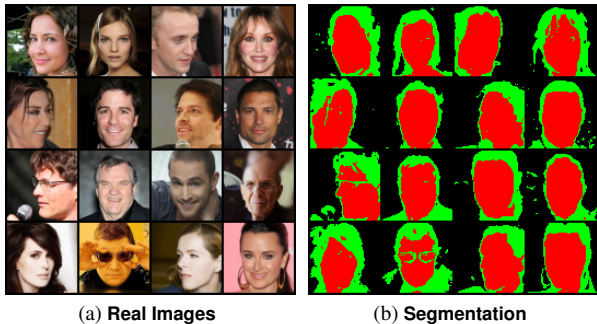


Figure 5. Segmentation on CelebA.

Methods	Acc.	mIOU
Supervised UNet	95.7	90.2
DatasetDDPM-unsup. [2]	78.5	69.3
Ours	87.9	80.3

Table 3. Segmentation comparisons on CelebA.

power to each individual image segment, which may benefit the denoising task during training. More importantly, our method can produce accurate corresponding masks, closely aligned with the semantic partitions in the generated image.

We evaluate the segmentation quality. Since there is no ground-truth mask provided for generated images, we apply the U-Net segmentation models (pre-trained on respective labeled training sets) to the generated images to produce reference masks. We measure the consistency between the reference and the predicted parsing results in terms of pixel-wise accuracy. We compare our method with a pre-

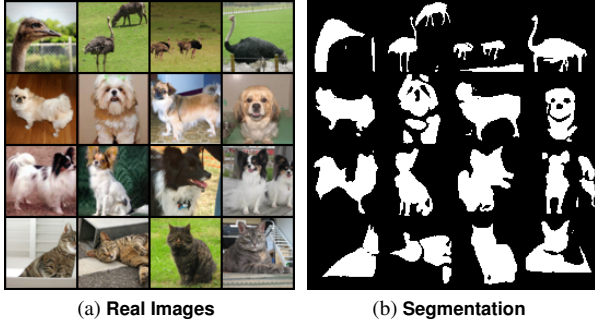


Figure 6. Segmentation on ImageNet.

Methods	Acc.	mIOU
Supervised UNet	85.7	74.1
DatasetDDPM-unsup. [2]	74.1	60.4
Ours	80.7	67.7

Table 4. Segmentation comparisons on ImageNet.

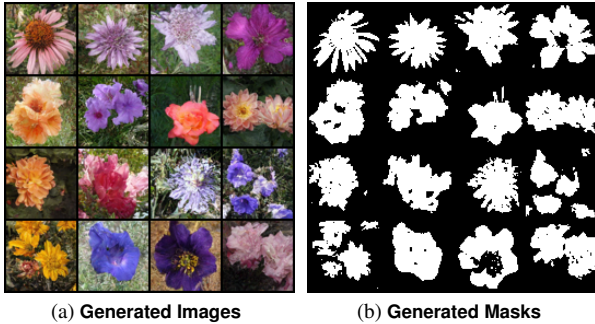


Figure 7. Generation on Flower.

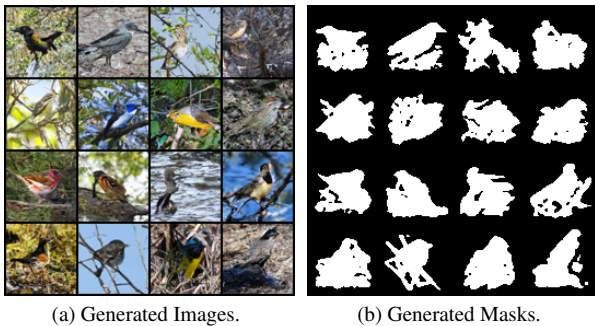


Figure 8. Generation on CUB.

trained DDPM baseline, in which we first perform image generation, then pass them to DatasetDDPM-unsup to get masks. As shown in Table 5 (bottom), our method consistently achieves better segmentation on generated images than the DDPM baseline. Note that, different from the two-stage baseline, our method performs the computation in a single stage, generating image and mask simultaneously. Appendix Section 6.2 shows more visualizations.

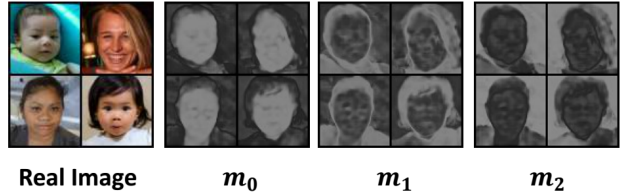


Figure 9. Mask factorization (3 parts) on FFHQ.

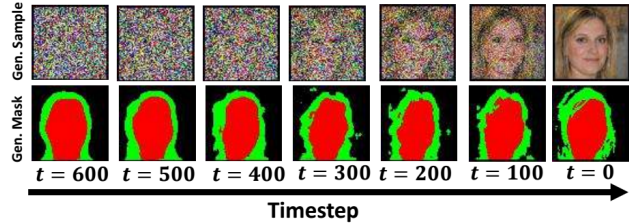


Figure 10. Generation refinement along diffusion.

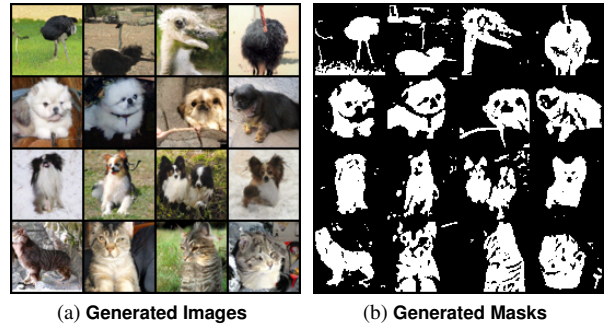


Figure 11. Conditional generation on ImageNet.

Methods	IOU.(↑)	FID (↓)
Concat	20.7	14.21
Masking h_{mid}	20.2	14.33
w/o weight sharing	50.5	17.21
Ours	56.1	10.28

Table 6. Ablations of decoding scheme on CUB.

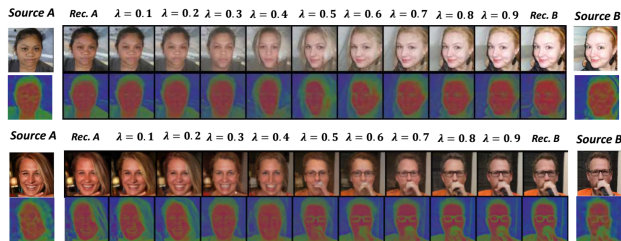


Figure 12. Interpolations of FFHQ with 250 timesteps of diffusion.

4.3. Ablation Study and Analysis

Multi-branch Decoders with Weight Sharing. Separating computation in multi-branch decoders with weight sharing is an essential design in our method. We show the effectiveness of this design by varying how to apply factor-

Table 5. Image and mask generation comparison on all datasets. (upper: FID(↓) bottom: Acc. (↑))

Models	Flower-64	Flower-128	CUB-64	CUB-128	FFHQ-64	FFHQ-128	ImageNet-64
DDPM	15.81	14.62	14.45	14.01	13.72	13.35	7.02
Ours	13.33	11.50	10.91	10.28	12.02	10.79	6.54
DDPM	80.5	82.9	84.2	83.7	84.2	84.2	71.2
Ours	92.3	92.7	91.4	91.2	90.3	90.7	84.1

ized masks in our decoding scheme: (1) concat: we use single branch to take concatenation of h and m . (2) masking h_{mid} : we use m to mask h_{mid} instead of h_{enc} . (3) w/o weight sharing: we train decoders separately in our design. Table 6 shows separate design consistently yields better visual features than other designs for CUB. This suggests that our design benefits from fully utilizing mask information in the end-to-end denoising task and avoids a trivial solution where masks are simply ignored.

Investigation on Mask Factorization. Our architecture is able to generate factorized representations, each representing a particular segment of the input image. We show this by visualizing the individual channels from softmax layer output in our mask generator. As shown in Figure 9, skin, hair, and background are separated in different channels.

Mask Refinement along Diffusion Process. In the DDPM Markov process, the model implicitly formulates a mapping between noise and data distributions. We validate that this occurs for both images and latent region masks by visualizing image and mask generation along the sequential reversed diffusion process in Figure 10. We observe gradual refinement as denoising steps approach $t = 0$.

Face Interpolation. We also investigate the face interpolation task on FFHQ. Similar to standard DDPM [25], we perform the interpolation in the denoising latent space with 250 timesteps of diffusion. Figure 12 shows good reconstruction in both pixels and region masks, yielding smoothly varying interpolations across face attributes such as pose, skin, hair, expression, and background.

Zero-shot Object Segmentation. We evaluate zero-shot object segmentation on both PASCAL VOC 2012 [15] and DAVIS-2017 videos [44]. Baseline DDPM generation is not solved for these datasets when training from scratch without external large-scale datasets (e.g., LAION [52] used in Stable Diffusion [47]). We directly adopt zero-shot transfer from our pre-trained ImageNet model by applying the conditional label mapping. We detail the mapping rule in Appendix Section 6.3. Figure 13 shows the accurate segmentation results for images of classes: aeroplane, monitor, person, and sofa from VOC. Since our method does not require any pixel labels, we evaluate the performance of each object class individually. Our method achieves a favorable high accuracy of **0.78** and mIOU of **0.54** when averaging over all 20 classes. We also report the results for each individual class in Appendix Section 6.4. We also show video



(a) Real Images (b) Segmentation
Figure 13. Segmentation on VOC-2012.



(a) Frames of 'Bear'



(b) Frames of 'Dog'

Figure 14. Segmentation on DAVIS-2017.

segmentation on DAVIS-2017 in Figure 14 and Appendix Section 6.5, without any labeled video pre-training.

5. Conclusion

We propose a factorized architecture for diffusion models that is able to perform unsupervised image segmentation and generation simultaneously, while being trained once, from scratch, for image generation via denoising alone. Using model architecture as a constraint, via carefully designed component factorization and parallel decoding schemes, our method effectively and efficiently bridges these two challenging tasks in a unified framework, without the need of fine-tuning or alternating the original DDPM training objective. Our work is the first example of engineering an architectural bottleneck so that learning a desired end task becomes a necessary byproduct of training to generate.

References

- [1] Pablo Arbeláez, Michael Maire, Charless Fowlkes, and Jitendra Malik. Contour detection and hierarchical image segmentation. *PAMI*, 2011.
- [2] Dmitry Baranchuk, Andrey Voynov, Ivan Rubachev, Valentin Khrulkov, and Artem Babenko. Label-efficient semantic segmentation with diffusion models. In *ICLR*, 2022.
- [3] Gedas Bertasius, Jianbo Shi, and Lorenzo Torresani. Deepedge: A multi-scale bifurcated deep network for top-down contour detection. In *CVPR*, 2015.
- [4] Adam Bielski and Paolo Favaro. Emergence of object segmentation in perturbed generative models. In *NeurIPS*, 2019.
- [5] John Canny. A computational approach to edge detection. *PAMI*, 1986.
- [6] Mathilde Caron, Piotr Bojanowski, Julien Mairal, and Armand Joulin. Unsupervised pre-training of image features on non-curated data. In *ICCV*, 2019.
- [7] Mathilde Caron, Hugo Touvron, Ishan Misra, Hervé Jégou, Julien Mairal, Piotr Bojanowski, and Armand Joulin. Emerging properties in self-supervised vision transformers. In *ICCV*, 2021.
- [8] Mickaël Chen, Thierry Artières, and Ludovic Denoyer. Unsupervised object segmentation by redrawing. In *NeurIPS*, 2019.
- [9] Ting Chen, Simon Kornblith, Mohammad Norouzi, and Geoffrey E. Hinton. A simple framework for contrastive learning of visual representations. *CoRR*, abs/2002.05709, 2020.
- [10] Xi Chen, Yan Duan, Rein Houthoofd, John Schulman, Ilya Sutskever, and Pieter Abbeel. Infogan: Interpretable representation learning by information maximizing generative adversarial nets. In *NeurIPS*, 2016.
- [11] Xinlei Chen, Haoqi Fan, Ross B. Girshick, and Kaiming He. Improved baselines with momentum contrastive learning. *CoRR*, abs/2003.04297, 2020.
- [12] Jia Deng, Wei Dong, Richard Socher, Li-Jia Li, Kai Li, and Fei-Fei Li. Imagenet: A large-scale hierarchical image database. In *CVPR*, 2009.
- [13] Lee Raymond Dice. Measures of the amount of ecologic association between species. *Ecology*, 1945.
- [14] Carl Doersch, Abhinav Gupta, and Alexei A. Efros. Unsupervised visual representation learning by context prediction. In *ICCV*, 2015.
- [15] M. Everingham, L. Van Gool, C. K. I. Williams, J. Winn, and A. Zisserman. The PASCAL Visual Object Classes Challenge 2012 (VOC2012) Results. <http://www.pascal-network.org/challenges/VOC/voc2012/workshop/index.html>.
- [16] Ross B. Girshick, Jeff Donahue, Trevor Darrell, and Jitendra Malik. Rich feature hierarchies for accurate object detection and semantic segmentation. In *CVPR*, 2014.
- [17] Ian J. Goodfellow, Jean Pouget-Abadie, Mehdi Mirza, Bing Xu, David Warde-Farley, Sherjil Ozair, Aaron C. Courville, and Yoshua Bengio. Generative adversarial nets. In *NeurIPS*, 2014.
- [18] Bharath Hariharan, Pablo Andrés Arbeláez, Ross B. Girshick, and Jitendra Malik. Hypercolumns for object segmentation and fine-grained localization. In *CVPR*, 2015.
- [19] Kaiming He, Xiangyu Zhang, Shaoqing Ren, and Jian Sun. Deep residual learning for image recognition. In *CVPR*, 2016.
- [20] Kaiming He, Georgia Gkioxari, Piotr Dollár, and Ross B. Girshick. Mask R-CNN. In *ICCV*, 2017.
- [21] Kaiming He, Haoqi Fan, Yuxin Wu, Saining Xie, and Ross B. Girshick. Momentum contrast for unsupervised visual representation learning. In *CVPR*, 2020.
- [22] Kaiming He, Xinlei Chen, Saining Xie, Yanghao Li, Piotr Dollár, and Ross B. Girshick. Masked autoencoders are scalable vision learners. In *CVPR*, 2022.
- [23] Martin Heusel, Hubert Ramsauer, Thomas Unterthiner, Bernhard Nessler, and Sepp Hochreiter. GANs trained by a two time-scale update rule converge to a local Nash equilibrium. In *NeurIPS*, 2017.
- [24] R. Devon Hjelm, Alex Fedorov, Samuel Lavoie-Marchildon, Karan Grewal, Philip Bachman, Adam Trischler, and Yoshua Bengio. Learning deep representations by mutual information estimation and maximization. In *ICLR*, 2019.
- [25] Jonathan Ho, Ajay Jain, and Pieter Abbeel. Denoising diffusion probabilistic models. In *NeurIPS*, 2020.
- [26] Gao Huang, Zhuang Liu, Laurens van der Maaten, and Kilian Q. Weinberger. Densely connected convolutional networks. In *CVPR*, 2017.
- [27] Jyh-Jing Hwang, Stella X. Yu, Jianbo Shi, Maxwell D. Collins, Tien-Ju Yang, Xiao Zhang, and Liang-Chieh Chen. Segsort: Segmentation by discriminative sorting of segments. In *ICCV*, 2019.
- [28] Xu Ji, Andrea Vedaldi, and João F. Henriques. Invariant information clustering for unsupervised image classification and segmentation. In *ICCV*, 2019.
- [29] Tero Karras, Samuli Laine, and Timo Aila. A style-based generator architecture for generative adversarial networks. In *CVPR*, 2019.
- [30] Diederik P. Kingma and Max Welling. Auto-encoding variational bayes. In *ICLR*, 2014.
- [31] Alexander Kirillov, Eric Mintun, Nikhila Ravi, Hanzi Mao, Chloe Rolland, Laura Gustafson, Tete Xiao, Spencer Whitehead, Alexander C. Berg, Wan-Yen Lo, Piotr Dollár, and Ross Girshick. Segment anything. *arXiv:2304.02643*, 2023.
- [32] Iasonas Kokkinos. Pushing the boundaries of boundary detection using deep learning. In *ICLR*, 2016.
- [33] Gustav Larsson, Michael Maire, and Gregory Shakhnarovich. Colorization as a proxy task for visual understanding. In *CVPR*, 2017.
- [34] Cheng-Han Lee, Ziwei Liu, Lingyun Wu, and Ping Luo. Maskgan: Towards diverse and interactive facial image manipulation. In *IEEE Conference on Computer Vision and Pattern Recognition (CVPR)*, 2020.
- [35] Ke Li and Jitendra Malik. Implicit maximum likelihood estimation. *CoRR*, abs/1809.09087, 2018.
- [36] Tianhong Li, Huiwen Chang, Shlok Kumar Mishra, Han Zhang, Dina Katabi, and Dilip Krishnan. MAGE: masked generative encoder to unify representation learning and image synthesis. *CoRR*, abs/2211.09117, 2022.
- [37] Tsung-Yi Lin, Michael Maire, Serge J. Belongie, James Hays, Pietro Perona, Deva Ramanan, Piotr Dollár, and

- C. Lawrence Zitnick. Microsoft COCO: common objects in context. In *ECCV*, 2014.
- [38] Wei Liu, Dragomir Anguelov, Dumitru Erhan, Christian Szegedy, Scott E. Reed, Cheng-Yang Fu, and Alexander C. Berg. SSD: single shot multibox detector. In *ECCV*, 2016.
- [39] Jonathan Long, Evan Shelhamer, and Trevor Darrell. Fully convolutional networks for semantic segmentation. In *CVPR*, 2015.
- [40] David Martin, Charless Fowlkes, Doron Tal, and Jitendra Malik. A database of human segmented natural images and its application to evaluating segmentation algorithms and measuring ecological statistics. *ICCV*, 2001.
- [41] David Martin, Charless Fowlkes, and Jitendra Malik. Learning to detect natural image boundaries using local brightness, color and texture cues. *PAMI*, 2004.
- [42] Maria-Elena Nilsback and Andrew Zisserman. Automated flower classification over a large number of classes. In *ICVGIP*, 2008.
- [43] Yassine Ouali, Céline Hudelot, and Myriam Tami. Autoregressive unsupervised image segmentation. In *ECCV*, 2020.
- [44] Jordi Pont-Tuset, Federico Perazzi, Sergi Caelles, Pablo Arbeláez, Alexander Sorkine-Hornung, and Luc Van Gool. The 2017 davis challenge on video object segmentation. *arXiv:1704.00675*, 2017.
- [45] Konpat Preechakul, Nattanat Chatthee, Suttisak Wizadwongsa, and Supasorn Suwajanakorn. Diffusion autoencoders: Toward a meaningful and decodable representation. In *CVPR*, 2022.
- [46] Joseph Redmon, Santosh Kumar Divvala, Ross B. Girshick, and Ali Farhadi. You only look once: Unified, real-time object detection. In *CVPR*, 2016.
- [47] Robin Rombach, Andreas Blattmann, Dominik Lorenz, Patrick Esser, and Björn Ommer. High-resolution image synthesis with latent diffusion models. In *CVPR*, 2022.
- [48] Olaf Ronneberger, Philipp Fischer, and Thomas Brox. U-Net: Convolutional networks for biomedical image segmentation. In *MICCAI*, 2015.
- [49] Carsten Rother, Vladimir Kolmogorov, and Andrew Blake. “GrabCut”: Interactive foreground extraction using iterated graph cuts. *ACM Trans. Graph.*, 2004.
- [50] Olga Russakovsky, Jia Deng, Hao Su, Jonathan Krause, Sanjeev Sathesh, Sean Ma, Zhiheng Huang, Andrej Karpathy, Aditya Khosla, Michael Bernstein, Alexander C. Berg, and Li Fei-Fei. ImageNet large scale visual recognition challenge. *IJCV*, 115(3):211–252, 2015.
- [51] Pedro Savarese, Sunnie S. Y. Kim, Michael Maire, Greg Shakhnarovich, and David McAllester. Information-theoretic segmentation by inpainting error maximization. In *CVPR*, 2021.
- [52] Christoph Schuhmann, Romain Beaumont, Richard Vencu, Cade Gordon, Ross Wightman, Mehdi Cherti, Theo Coombes, Aarush Katta, Clayton Mullis, Mitchell Wortsman, Patrick Schramowski, Srivatsa Kundurthy, Katherine Crowson, Ludwig Schmidt, Robert Kaczmarczyk, and Jenia Jitsev. LAION-5B: an open large-scale dataset for training next generation image-text models. In *NeurIPS*, 2022.
- [53] Wei Shen, Xinggang Wang, Yan Wang, Xiang Bai, and Zhijiang Zhang. Deepcontour: A deep convolutional feature learned by positive-sharing loss for contour detection. In *CVPR*, 2015.
- [54] Jianbo Shi and Jitendra Malik. Normalized cuts and image segmentation. *PAMI*, 2000.
- [55] Karen Simonyan and Andrew Zisserman. Very deep convolutional networks for large-scale image recognition. In *ICLR*, 2015.
- [56] Jiaming Song, Chenlin Meng, and Stefano Ermon. Denoising diffusion implicit models. In *ICLR*, 2021.
- [57] Aaron van den Oord, Nal Kalchbrenner, Oriol Vinyals, Lasse Espeholt, Alex Graves, and Koray Kavukcuoglu. Conditional image generation with PixelCNN decoders. In *NeurIPS*, 2016.
- [58] C. Wah, S. Branson, P. Welinder, P. Perona, and S. Belongie. The Caltech-UCSD Birds-200-2011 Dataset. Technical Report CNS-TR-2011-001, California Institute of Technology, 2011.
- [59] Weijia Wu, Yuzhong Zhao, Mike Zheng Shou, Hong Zhou, and Chunhua Shen. Diffumask: Synthesizing images with pixel-level annotations for semantic segmentation using diffusion models. *ICCV*, 2023.
- [60] Saining Xie and Zhuowen Tu. Holistically-nested edge detection. In *ICCV*, 2015.
- [61] Tao Xu, Pengchuan Zhang, Qiuyuan Huang, Han Zhang, Zhe Gan, Xiaolei Huang, and Xiaodong He. AttnGAN: Fine-grained text to image generation with attentional generative adversarial networks. In *CVPR*, 2018.
- [62] Han Zhang, Tao Xu, Hongsheng Li, Shaoting Zhang, Xiaogang Wang, Xiaolei Huang, and Dimitris Metaxas. StackGAN: Text to photo-realistic image synthesis with stacked generative adversarial networks. In *ICCV*, 2017.
- [63] Richard Zhang, Phillip Isola, and Alexei A. Efros. Colorful image colorization. In *ECCV*, 2016.
- [64] Shiyin Zhang, Jun Hao Liew, Yunchao Wei, Shikui Wei, and Yao Zhao. Interactive object segmentation with inside-outside guidance. In *CVPR*, 2020.
- [65] Xiao Zhang and Michael Maire. Self-supervised visual representation learning from hierarchical grouping. In *NeurIPS*, 2020.
- [66] Zijian Zhang, Zhou Zhao, and Zhijie Lin. Unsupervised representation learning from pre-trained diffusion probabilistic models. In *NeurIPS*, 2022.

6. Appendix

6.1. Additional Segmentation Results

We show more segmentation results for Flower, CUB, FFHQ, CelebA and ImageNet. As shown in Figures 15, 16, 17, 18, and 19, our method consistently predicts accurate segmentations for real image inputs.

6.2. Additional Generation Results

We show more generation results for Flower, CUB, FFHQ, and ImageNet (classes: flamingo, water buffalo, garbage truck, and sports car). As shown in Figures 20, 21, 22, and 23, our method consistently produces images and masks with high quality.

ImageNet cls.	Num of VOC val image	
1:aeroplane	895:warplane	136
2:bicycle	671:mountain-bike	108
3:bird	94:hummingbird	168
4:boat	814:speedboat	115
5:bottle	907:wine-bottle	133
6:bus	779:school-bus	114
7:car	817:sports-car	191
8:cat	281:tabby	206
9:chair	765:rocking-chair	175
10:cow	346:water-buffalo	102
11:diningtable	532:dining-table	89
12:dog	153:maltese-dog	204
13:horse	603:horsecart	104
14:motorbike	670:motorscooter	117
15:person	981:ballplayer	584
16:potted plant	883:vase	116
17:sheep	348:ram	89
18:sofa	831:studio-couch	109
19:train	466:bullet-train	126
20:tv/monitor	664:monitor	106

Table 7. Class label mapping from ImageNet to VOC.

6.3. Label Mapping for Zero-shot Transfer

At the current stage of diffusion model research, generation is not solved for PASCAL VOC when training from scratch without an external large-scale dataset (*e.g.*, LAION used in stable diffusion). There is no baseline DDPM model that can achieve this. As such, we adopt our conditional ImageNet model to perform zero-shot segmentation on VOC by mapping class labels from ImageNet to VOC. Table 7 details the mapping rule.

6.4. Additional Zero-shot Results on VOC

We report pixel accuracy and mIOU of each class in VOC in Table 8, which demonstrates that our method can achieve

VOC cls.	Acc.	mIOU
1:aeroplane	0.82	0.57
2:bicycle	0.79	0.47
3:bird	0.83	0.58
4:boat	0.81	0.51
5:bottle	0.76	0.47
6:bus	0.73	0.54
7:car	0.74	0.48
8:cat	0.82	0.66
9:chair	0.75	0.64
10:cow	0.82	0.45
11:diningtable	0.69	0.62
12:dog	0.82	0.67
13:horse	0.84	0.53
14:motorbike	0.76	0.52
15:person	0.77	0.46
16:potted plant	0.74	0.46
17:sheep	0.84	0.64
18:sofa	0.73	0.51
19:train	0.76	0.56
20:tv/monitor	0.73	0.47
average	0.78	0.54

Table 8. Accuracy and mIOU per class in VOC.

reasonable high performance. We also provide more segmentation results of ‘bicycle’, ‘chair’, ‘potted plant’ and ‘train’ in Figure 24.

6.5. Additional Zero-shot Results on DAVIS

We provide more DAVIS-2017 video segmentation results of ‘classic-car’, ‘dance-jump’ in Figure 25.

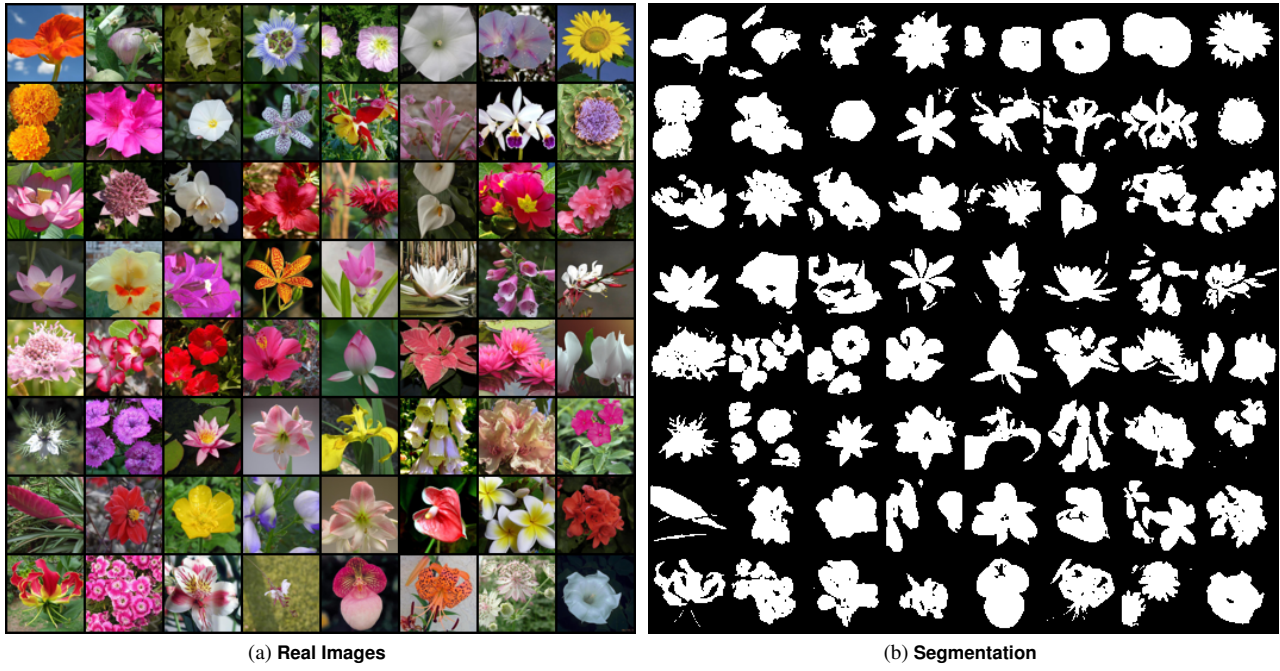


Figure 15. Segmentation on Flower.

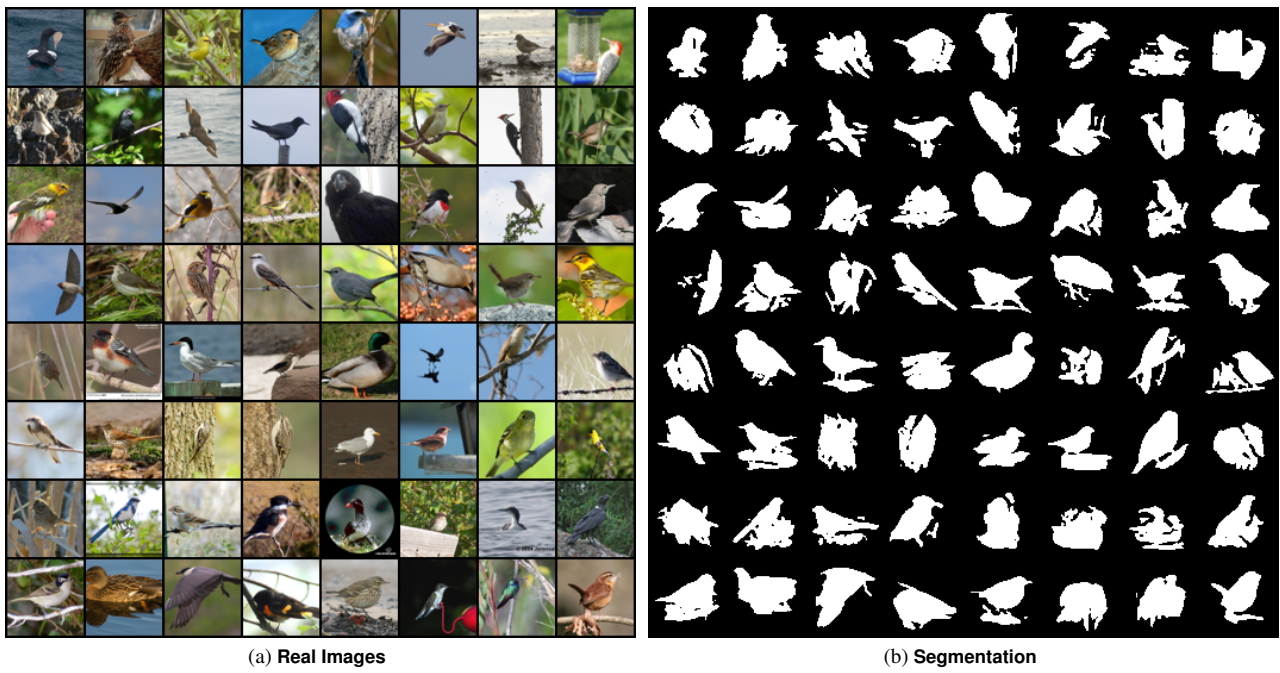


Figure 16. Segmentation on CUB.

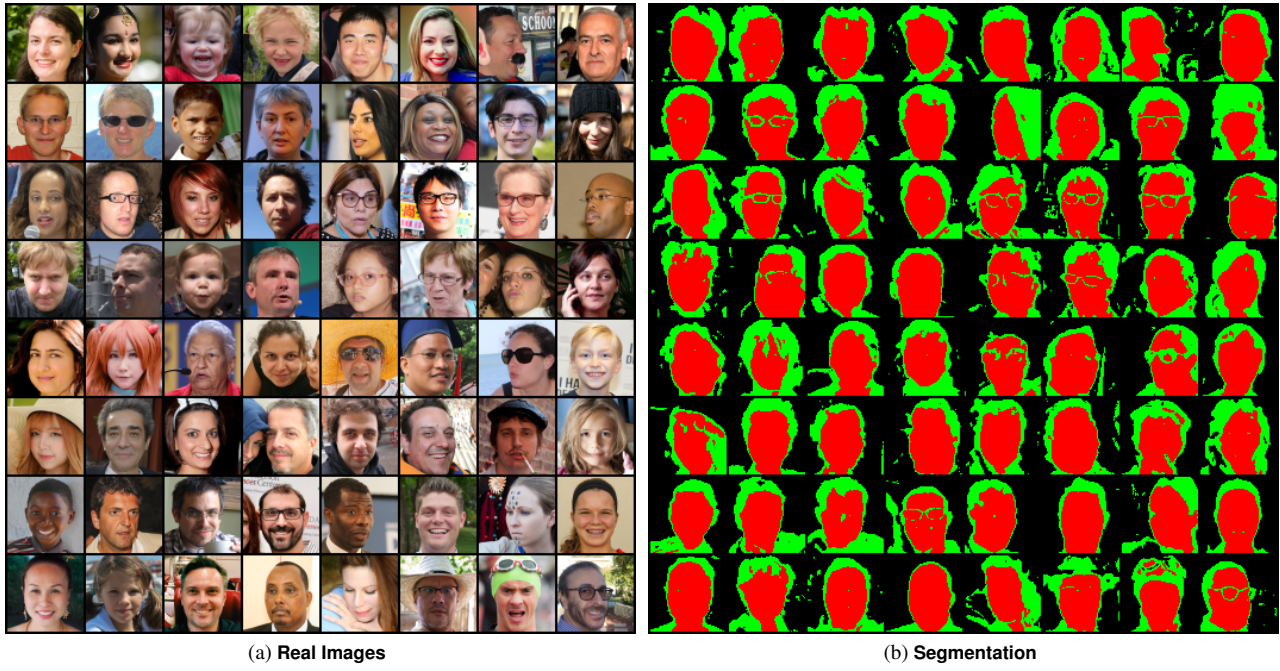


Figure 17. Segmentation on FFHQ.

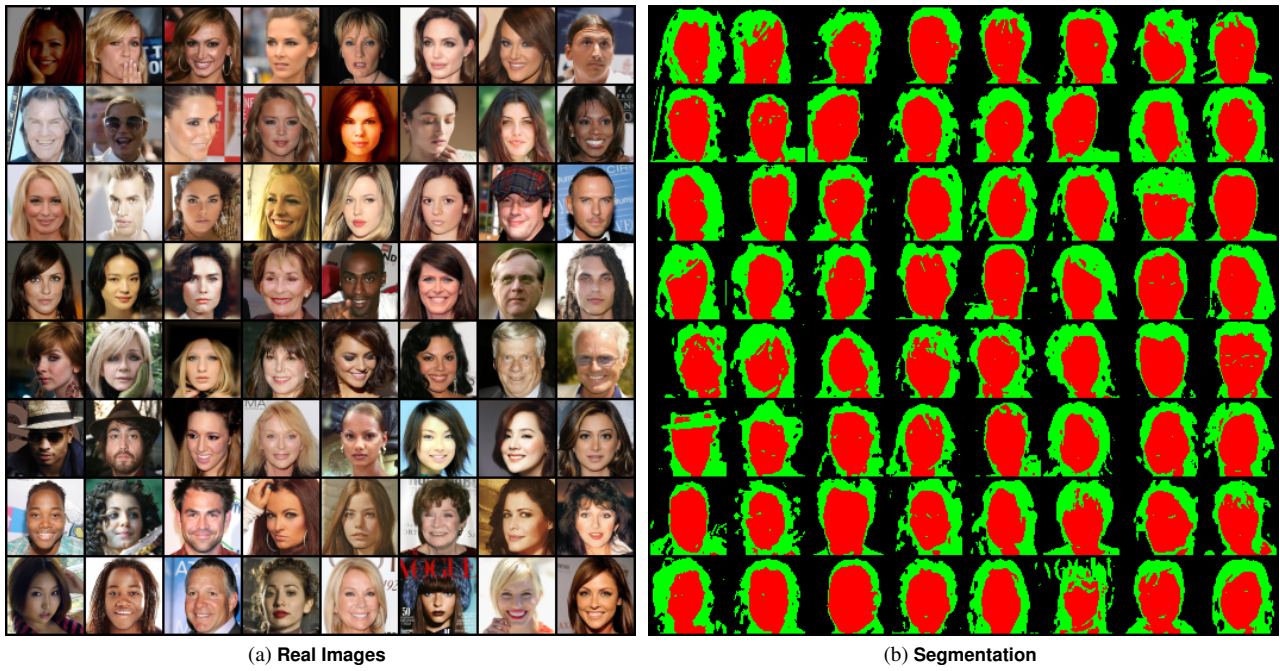
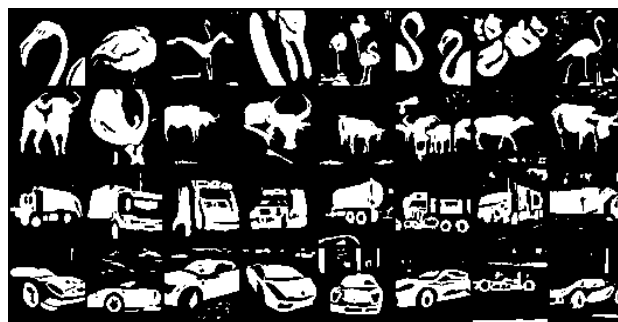


Figure 18. Segmentation on CelebA.

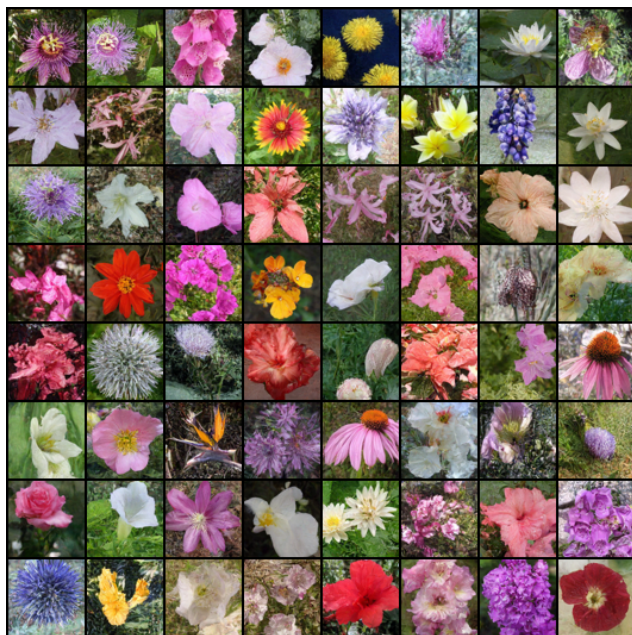


(a) Real Images

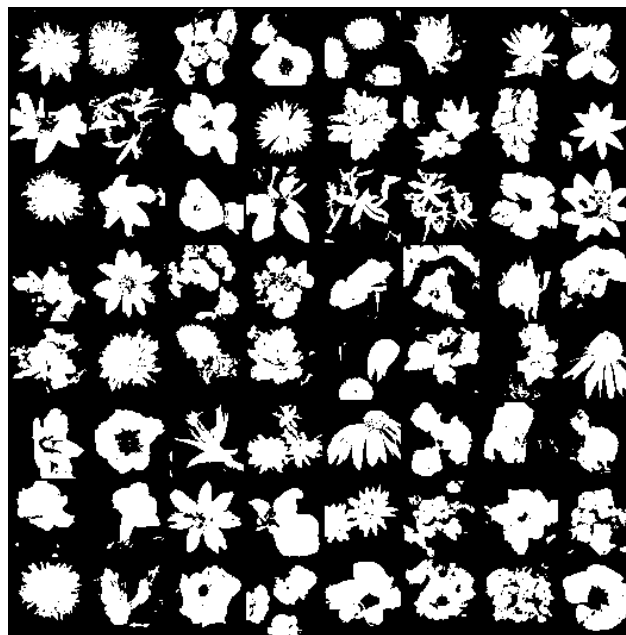


(b) Segmentation

Figure 19. Segmentation on ImageNet.



(a) Generated Images



(b) Generated Masks

Figure 20. Generation on Flower.

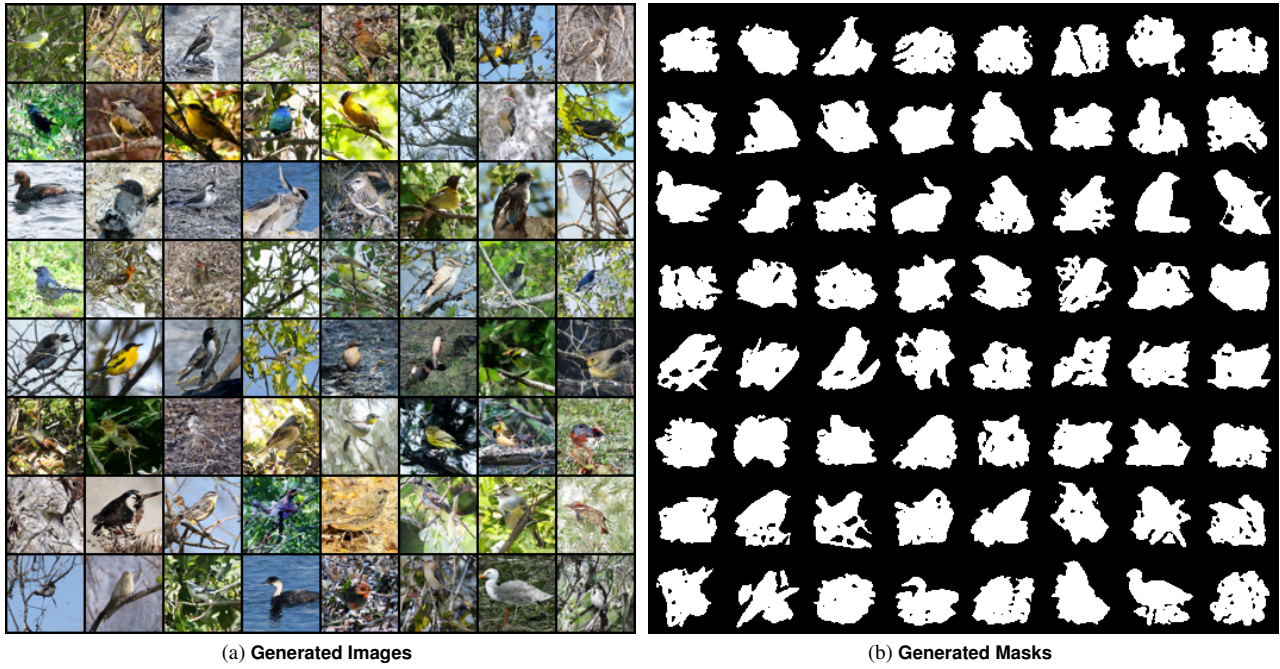


Figure 21. Generation on CUB.

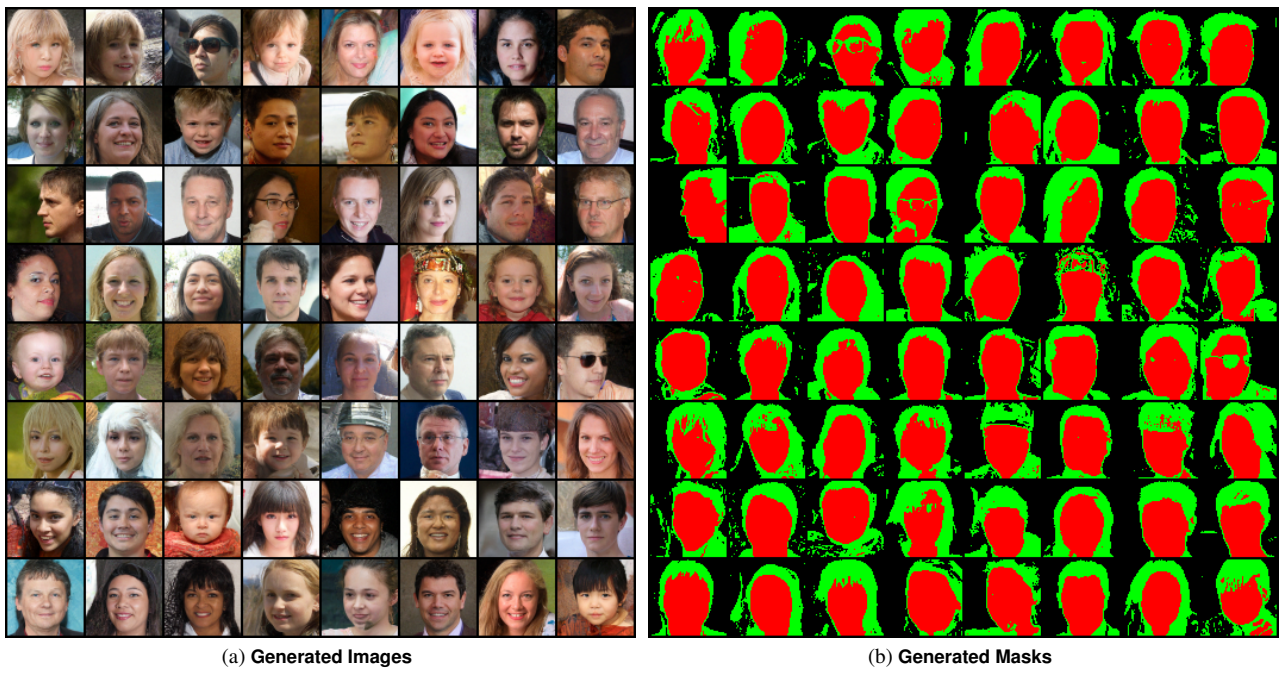


Figure 22. Generation on FFHQ.

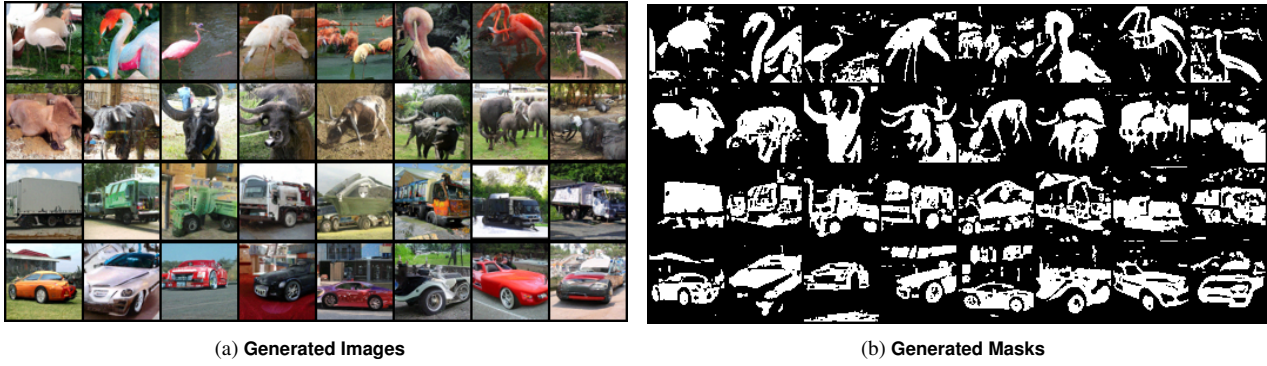


Figure 23. Conditional ImageNet generation.

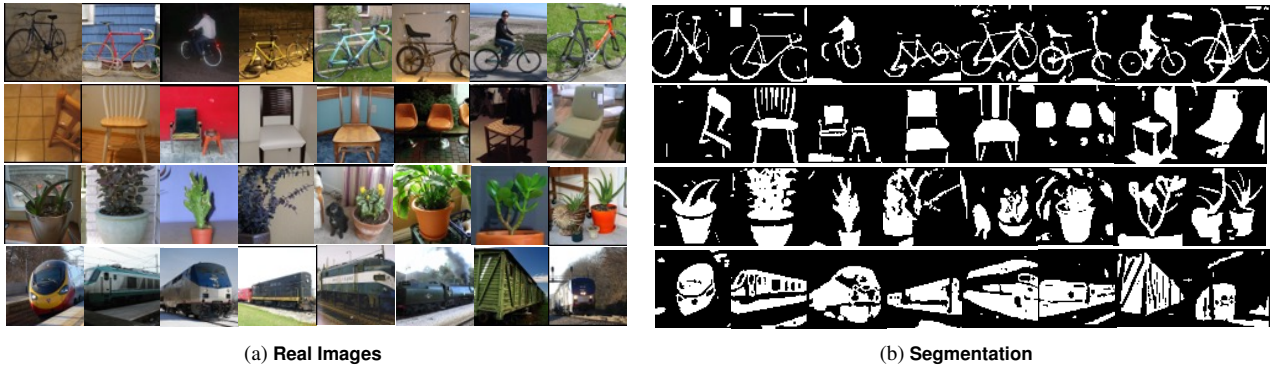


Figure 24. Segmentation on VOC-2012.

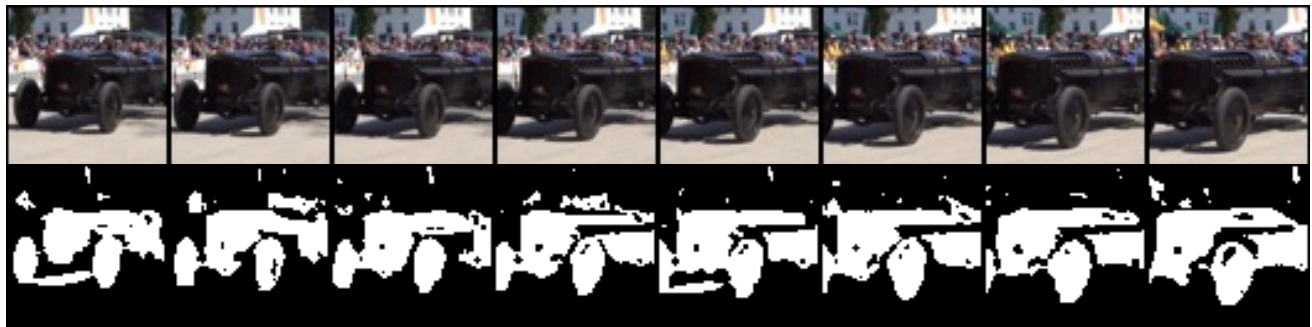


Figure 25. Segmentation on DAVIS-2017.